

FAST HADRON FREEZE-OUT GENERATOR, PART II: NONCENTRAL COLLISIONS.

N.S. Amelin* and R. Lednicky[†]

*Joint Institute for Nuclear Research,
Dubna, Moscow Region, 141980, Russia*

I.P. Lokhtin, L.V. Malinina,[‡] and A.M. Snigirev

*M.V. Lomonosov Moscow State University,
D.V. Skobeltsyn Institute of Nuclear Physics, 119991, Moscow, Russia*

Iu.A. Karpenko and Yu.M. Sinyukov

Bogolyubov Institute for Theoretical Physics, Kiev, 03143, Ukraine

I. Arsene[§] and L. Bravina

The department of Physics, University of Oslo, Norway

(Dated: February 9, 2022)

Abstract

The fast Monte Carlo procedure of hadron generation developed in our previous work is extended to describe noncentral collisions of nuclei. We consider different possibilities to introduce appropriate asymmetry of the freeze-out hyper-surface and flow velocity profile. For comparison with other models and experimental data we demonstrate the results based on the standard parametrizations of the hadron freeze-out hyper-surface and flow velocity profile assuming either a common chemical and thermal freeze-out or the chemically frozen evolution from chemical to thermal freeze-out. The C++ generator code is written under the ROOT framework and is available for public use at <http://uhkm.jinr.ru/>.

PACS numbers: 25.75.Dw, 24.10.Lx, 25.75.Gz

*deceased

[†]Also at Institute of Physics AS CR, 18221 Praha 8, Czech Republic

[‡]Also at Joint Institute for Nuclear Research, Dubna, Moscow Region, 141980, Russia

[§]Also at Institute for Space Sciences, Bucharest-Magurele, Romania

I. INTRODUCTION

In the preceding work [1] we have developed a Monte Carlo (MC) simulation procedure, and the corresponding C++ code allowing for a fast but realistic description of multiple hadron production in central relativistic heavy ion collisions. A high generation speed and easy control through input parameters make our MC generator code particularly useful for detector studies. The generator code is quite flexible and allows the user to add other scenarios and freeze-out surface parametrizations as well as additional hadron species in a simple manner. We have compared the BNL Relativistic Heavy Ion Collider (RHIC) experimental data on central Au+Au collisions with our MC generation results obtained within the single freeze-out scenario with Bjorken-like and Hubble-like freeze-out surface parametrizations. Although simplified, such a scenario nevertheless allowed for a reasonable description of particle spectra and femtoscopic momentum correlations. This description can be farther improved by introducing finite emission duration and extending the table of the included resonances; the single freeze-out scenario is however less successful in the description of the data on elliptic flow (see section III).

The particle densities at the chemical freeze-out stage are too high (see, e.g., [2]) to consider particles as free streaming and to associate this stage with the thermal freeze-out one. In this work we have implemented as an option more sophisticated scenario of thermal freeze-out: the system expands hydrodynamically with frozen chemical composition, cools down and finally decays at some thermal freeze-out hypersurface. The RHIC experimental data are compared with our MC generation results obtained within this thermal freeze-out scenario. We do not consider here a more complex freeze-out scenario taking into account continuous particle emission (see, e.g., [3]).

In present paper, we also extend the fast Monte Carlo procedure of hadron generation developed in our previous work [1] to describe noncentral collisions of nuclei. One of the most spectacular features of the RHIC data is large elliptic flow [4]. The development of a strong flow is well described by the hydrodynamic models and requires short time scale and large pressure gradients, attributed to strongly interacting systems. However, results of hydrodynamic models significantly disagree with the data on femtoscopic momentum correlations (compare [5] with, e.g., [6]), related with the space-time characteristics of the system at freeze-out. Usually, the hadronic cascade models underestimate the momentum

anisotropy and overestimate the source sizes (e.g. [7, 8, 9]). Some sophisticated hybrid models (e.g. AMPT [10]) reproduce the elliptic flow and the correlation radii but with different sets of model parameters.

Successful attempts to describe simultaneously the momentum-space measurements and the freeze-out coordinate-space data were done in several models which make experimental data fitting within some parametrizations of freeze-out hypersurface: “Kiev-Nantes” model [3], “Blast-Wave” parametrizations [11, 12, 13], “Buda-Lund” hydro approach [14]. All these approaches use the hydro-inspired parametrizations of freeze-out hypersurface and help in understanding the full freeze-out scenario at RHIC.

In this article we analyze the RHIC data at $\sqrt{s_{NN}} = 200$ GeV and try to use the same set of the model parameters for the description of both the momentum-space observables, i.e. transverse mass (m_t) spectra and p_t -dependence of elliptic flow, and freeze-out coordinate-space observables, i.e. k_t -dependence and azimuthal angle (Φ) dependence of the correlation radii. The chemical composition of the fireball was fixed in our previous article [1] by the particle ratios analysis.

The paper is organized as follows. Section II is devoted to the description of main modifications of the model [1] needed to take into consideration noncentral collisions. In section III the example calculations are compared with the RHIC experimental data. We summarize and conclude in section IV.

II. FREEZE-OUT SURFACE PARAMETRIZATIONS

The extension of our MC generator to noncentral collisions demands mainly the modifications of freeze-out hypersurface parametrizations (Sec. V of Ref. [1]) and does not practically influence the generation procedure itself (Sec. VI of Ref. [1]). Therefore we focus on these modifications only considering the popular Bjorken-like and Hubble-like freeze-out parametrizations respectively used in so-called blast wave [11] and Cracow [15] models as the example options in our MC generator. Similar parametrizations have been used in the hadron generator THERMINATOR [12].

As usual, in the Bjorken-like parametrization, we substitute the Cartesian coordinates t ,

z by the Bjorken ones [16]

$$\tau = (t^2 - z^2)^{1/2}, \quad \eta = \frac{1}{2} \ln \frac{t+z}{t-z}, \quad (1)$$

and introduce the the radial vector $\vec{r} \equiv \{x, y\} = \{r \cos \phi, r \sin \phi\}$, i.e.,

$$x^\mu = \{\tau \cosh \eta, \vec{r}, \tau \sinh \eta\} = \{\tau \cosh \eta, r \cos \phi, r \sin \phi, \tau \sinh \eta\}. \quad (2)$$

For a freeze-out hypersurface represented by the equation $\tau = \tau(\eta, r, \phi)$, the hypersurface element in terms of the coordinates η, r, ϕ becomes

$$d^3\sigma_\mu = \epsilon_{\mu\alpha\beta\gamma} \frac{dx^\alpha dx^\beta dx^\gamma}{d\eta dr d\phi} d\eta dr d\phi, \quad (3)$$

where $\epsilon_{\mu\alpha\beta\gamma}$ is the completely antisymmetric Levy-Civita tensor in four dimensions with $\epsilon^{0123} = -\epsilon_{0123} = 1$. Generally, the freeze-out hypersurface is represented by a set of equations $\tau = \tau_j(\eta, r, \phi)$ and Eq. (3) should be substituted by the sum of the corresponding hypersurface elements. For the simplest and frequently used freeze-out hypersurface $\tau = \text{const}$, one has

$$\begin{aligned} d^3\sigma_\mu &= n_\mu d^3\sigma = \tau d^2\vec{r} d\eta \{\cosh \eta, 0, 0, -\sinh \eta\}, \\ d^3\sigma &= \tau d^2\vec{r} d\eta, \\ n^\mu &= \{\cosh \eta, 0, 0, \sinh \eta\}. \end{aligned} \quad (4)$$

In noncentral collisions the shape of the emission region in the transverse (x - y) plane can be approximated by an ellipse (as usual, the z - x plane coincides with the reaction plane). The ellipse radii $R_x(b)$ and $R_y(b)$ at a given impact parameter b are usually parametrized [11, 17, 18, 19] in terms of the spatial anisotropy $\epsilon(b) = (R_y^2 - R_x^2)/(R_x^2 + R_y^2)$ and the scale factor $R_s(b) = [(R_x^2 + R_y^2)/2]^{1/2}$,

$$R_x(b) = R_s(b) \sqrt{1 - \epsilon(b)}, \quad R_y(b) = R_s(b) \sqrt{1 + \epsilon(b)}. \quad (5)$$

Then from the ellipse equation,

$$\frac{x^2}{R_x^2} + \frac{y^2}{R_y^2} = 1, \quad (6)$$

follows the explicit dependence of the fireball transverse radius $R(b, \phi)$ on the azimuthal angle ϕ :

$$R(b, \phi) = R_s(b) \frac{\sqrt{1 - \epsilon^2(b)}}{\sqrt{1 + \epsilon(b) \cos 2\phi}}; \quad (7)$$

particularly, $R(b, 0) = R_x(b)$ and $R(b, \pi/2) = R_y(b)$. To reduce the number of free parameters, we assume here a simple scaling option [20]

$$R_s(b) = R_s(b=0)\sqrt{1 - \epsilon_s(b)}, \quad (8)$$

where $R_s(b=0) \equiv R$ is the fireball freeze-out transverse radius in central collisions. It means that the dimensionless ratio $R_s(b)/R_s(0)$ at the freeze-out moment depends on the collision energy, the radius R_A of the colliding (identical) nuclei and the impact parameter b through a dimensionless $\epsilon_s(b)$ only. It should be noted that both $\epsilon_s(b)$ and the fireball freeze-out eccentricity $\epsilon(b)$ are determined by the eccentricity $\epsilon_0(b) = b/(2R_A)$ of the elliptical overlap of the colliding nuclei at the initial moment, when

$$\left. \frac{R_s(b)}{R_s(b=0)} \right|_{\epsilon(b)=\epsilon_0(b)} \equiv \frac{R_s(b)_{\text{initial}}}{R_A} = \sqrt{1 - \epsilon_0(b)}. \quad (9)$$

Since $\epsilon_s(0) = \epsilon(0) = \epsilon_0(0) = 0$, one can assume that $\epsilon_s(b) \simeq \epsilon(b)$ at sufficiently small values of the impact parameter b . It appears that the use of the simple ansatz $\epsilon_s(b) = \epsilon(b)$ allows one to achieve the absolute normalization of particle spectra correct within $\sim 10\%$ up to $b \simeq R_A$ (see section III C).

If the system evolution were driven by the pressure gradients, the expansion would be stronger in the direction of the short ellipse x -axis (in the reaction plane), where the pressure gradient is larger than in the direction of the long ellipse y -axis (see, e.g., [6]). The typical hydrodynamic evolution scenario is shown in Fig. 1. During the evolution, the initial system coordinate anisotropy $\epsilon_0(b)$ is transformed into the momentum anisotropy $\delta(b)$. According to the hydrodynamical calculations, the spatial eccentricity almost disappears and the momentum anisotropy saturates at rather early evolution stage before freeze-out. As we do not trace the evolution here, we will consider the spatial and momentum anisotropies $\epsilon(b)$ and $\delta(b)$ as free parameters.

For central collisions the fluid flow four-velocity $u^\mu(t, \vec{x}) = \gamma(t, \vec{x})\{1, \vec{v}(t, \vec{x})\} \equiv \gamma(t, \vec{x})\{1, \vec{v}_\perp(t, \vec{x}), v_z(t, \vec{x})\}$ at a point \vec{x} and time t was parametrized [1] in terms of the longitudinal (z) and transverse (\perp) fluid flow rapidities

$$\eta_u(t, \vec{x}) = \frac{1}{2} \ln \frac{1 + v_z(t, \vec{x})}{1 - v_z(t, \vec{x})}, \quad \rho_u(t, \vec{x}) = \frac{1}{2} \ln \frac{1 + v_\perp(t, \vec{x}) \cosh \eta_u(t, \vec{x})}{1 - v_\perp(t, \vec{x}) \cosh \eta_u(t, \vec{x})}, \quad (10)$$

where $v_\perp = |\vec{v}_\perp|$ is the magnitude of the transverse component of the flow three-velocity

$\vec{v} = \{v_\perp \cos \phi_u, v_\perp \sin \phi_u, v_z\}$, i.e.,

$$\begin{aligned} u^\mu(t, \vec{x}) &= \{\cosh \rho_u \cosh \eta_u, \sinh \rho_u \cos \phi_u, \sinh \rho_u \sin \phi_u, \cosh \rho_u \sinh \eta_u\} \\ &= \{(1 + u_\perp^2)^{1/2} \cosh \eta_u, \vec{u}_\perp, (1 + u_\perp^2)^{1/2} \sinh \eta_u\}, \end{aligned} \quad (11)$$

$\vec{u}_\perp = \gamma \vec{v}_\perp = \gamma_\perp \cosh \eta_u \vec{v}_\perp$, $\gamma_\perp = \cosh \rho_u$. However, unlike the transverse isotropic parametrization ($\phi_u = \phi$), now the azimuthal angle ϕ_u of the fluid velocity vector is not necessarily identical to the spatial azimuthal angle ϕ , because of the nonzero flow anisotropy parameter $\delta(b)$ [18, 19] :

$$\begin{aligned} u^\mu(t, \vec{x}) &= \{\gamma_\phi \cosh \tilde{\rho}_u \cosh \eta_u, \sqrt{1 + \delta(b)} \sinh \tilde{\rho}_u \cos \phi, \\ &\quad \sqrt{1 - \delta(b)} \sinh \tilde{\rho}_u \sin \phi, \gamma_\phi \cosh \tilde{\rho}_u \sinh \eta_u\}, \end{aligned} \quad (12)$$

where

$$\gamma_\phi = \sqrt{1 + \delta(b) \tanh^2 \tilde{\rho}_u \cos 2\phi}, \quad (13)$$

$$\tan \phi_u = \sqrt{\frac{1 - \delta(b)}{1 + \delta(b)}} \tan \phi. \quad (14)$$

The transverse flow rapidity ρ_u is related to $\tilde{\rho}_u$ by:

$$u_\perp = \sinh \rho_u = \sqrt{1 + \delta(b) \cos 2\phi} \sinh \tilde{\rho}_u. \quad (15)$$

Note, that for $\delta(b) = 0$ (i.e. $\phi_u = \phi$), Eq. (12) reduces to Eq. (11) which was applied in Refs. [20, 21]. In Ref. [19], $\delta(b)$ is obtained by fitting the model prediction to the measured elliptic flow coefficient v_2 .

Further we assume the longitudinal boost invariance [16] $\eta_u = \eta$, which is a good approximation for the highest RHIC energies at the midrapidity region. To account for the violation of the boost invariance, we have also included in the code an option corresponding to the substitution of the uniform distribution of the space-time longitudinal rapidity η in the interval $[-\eta_{\max}, \eta_{\max}]$ by a Gaussian distribution $\exp(-\eta^2/2\Delta\eta^2)$ with a width parameter $\Delta\eta = \eta_{\max}$. The presence of the “oscillation term” $\sqrt{1 + \delta(b) \cos 2\phi}$ in the transverse component u_\perp of the flow velocity in Eq. (15) allows us to use the simple linear profile for $\tilde{\rho}_u$ without introduction of the additional parameters for each centrality (b) unlike other models, namely:

$$\tilde{\rho}_u = \frac{r}{R_s(b)} \rho_u^{\max}(b=0), \quad (16)$$

where $\rho_u^{\max}(b=0)$ is the maximal transverse flow rapidity for central collisions. At such normalization and $\delta(b) > \epsilon(b)$ the maximal transverse flow (u_\perp, ρ_u) is achieved at $\phi = 0$,

i.e. along x -axis as it should be according to the hydrodynamic scenario described above (Fig. 1). (although $\tilde{\rho}_u$ has a maximum at $\phi = \pi/2$!)

Here one should note that the “popular parametrization” of transverse flow rapidity used in Ref. [11] (and implemented as an option in our MC generator also):

$$\rho_u = \tilde{r}[\rho_0(b) + \rho_2(b) \cos 2\phi_u], \quad (17)$$

where

$$\tilde{r} \equiv \sqrt{\left(\frac{r \cos \phi}{R_x}\right)^2 + \left(\frac{r \sin \phi}{R_y}\right)^2} = \frac{r}{R(b, \phi)} \quad (18)$$

is the “normalized elliptical radius”, $\rho_0(b)$ and $\rho_2(b)$ are the two fitting parameters, is close to our parametrization and gives the similar results for observables under consideration. In parametrization of Ref. [11] the boost is perpendicular to the elliptical subshell on which the source element is found: $\tan \phi_u = (R_x^2/R_y^2) \tan \phi = (1 - \epsilon)/(1 + \epsilon) \tan \phi$ and $\delta(b) = 2\epsilon(b)/(1 + \epsilon^2(b))$. It is interesting to note that for sufficiently weak transverse flows, $\rho_u \leq 1$, considered here, one can put $\sinh \rho_u \simeq \rho_u$ and obtain our parametrization from that of Ref. [11] by substitutions

$$\frac{\rho_0(b)}{R(b, \phi)} \rightarrow \frac{\rho_u^{\max}(b=0)}{R_s(b)} \quad 1 + \frac{\rho_2(b)}{\rho_0(b)} \cos 2\phi_u \rightarrow \sqrt{1 + \delta(b) \cos 2\phi}. \quad (19)$$

Thus, in the case of moderate transverse flows, one can obtain the same result either by fixing the direction of the flow velocity vector but allowing for the azimuthal dependence of the flow rapidity or by allowing for arbitrary direction of the flow velocity vector but assuming azimuthally independent flow rapidity.

At $\tau = \text{const}$, the total effective volume for particle production in the case of noncentral collisions becomes

$$V_{\text{eff}} = \int_{\sigma(t, \vec{x})} d^3\sigma_\mu(t, \vec{x}) u^\mu(t, \vec{x}) = \tau \int_0^{2\pi} d\phi \int_0^{R(b, \phi)} (n_\mu u^\mu) r dr \int_{\eta_{\min}}^{\eta_{\max}} d\eta, \quad (20)$$

where $(n_\mu u^\mu) = \cosh \tilde{\rho}_u \sqrt{1 + \delta(b) \tanh^2 \tilde{\rho}_u \cos 2\phi}$.

We also consider the Cracow model scenario [15] corresponding to the Hubble-like freeze-out hypersurface $\tau_H = (t^2 - x^2 - y^2 - z^2)^{1/2} = \text{const}$. Introducing the longitudinal space-time rapidity η according to Eq. (1) and the transverse space-time rapidity $\rho = \sinh^{-1}(r/\tau_H)$, one has [22]

$$x^\mu = \tau_H \{\cosh \eta \cosh \rho, \sinh \rho \cos \phi, \sinh \rho \sin \phi, \sinh \eta \cosh \rho\}, \quad (21)$$

$\tau_H = \tau_B / \cosh \rho$. Representing the freeze-out hypersurface by the equation $\tau_H = \tau_H(\eta, \rho, \phi) = \text{const}$, one finds from Eq. (3):

$$\begin{aligned} d^3\sigma &= \tau_H^3 \sinh \rho \cosh \rho d\eta d\rho d\phi = \tau_H d\eta d^2\vec{r}, \\ n^\mu(t, \vec{x}) &= x^\mu(t, \vec{x}) / \tau_H. \end{aligned} \quad (22)$$

With the additional flow anisotropy parameter $\delta(b)$ the flow four-velocity is parametrized as [19]:

$$\begin{aligned} u^\mu(t, \vec{x}) &= \{\gamma_\phi^H \cosh \rho \cosh \eta, \sqrt{1 + \delta(b)} \sinh \rho \cos \phi, \\ &\quad \sqrt{1 - \delta(b)} \sinh \rho \sin \phi, \gamma_\phi^H \cosh \rho \sinh \eta\}, \end{aligned} \quad (23)$$

where

$$\gamma_\phi^H = \sqrt{1 + \delta(b) \tanh^2 \rho \cos 2\phi}. \quad (24)$$

The effective volume corresponding to $r = \tau_H \sinh \rho < R(b, \phi)$ and $\eta_{\min} \leq \eta \leq \eta_{\max}$ is

$$V_{\text{eff}} = \int_{\sigma(t, \vec{x})} d^3\sigma_\mu(t, \vec{x}) u^\mu(t, \vec{x}) = \tau_H \int_0^{2\pi} d\phi \int_0^{R(b, \phi)} (n_\mu u^\mu) r dr \int_{\eta_{\min}}^{\eta_{\max}} d\eta \quad (25)$$

with

$$\begin{aligned} (n_\mu u^\mu) &= \cosh^2 \rho \left(\sqrt{1 + \delta(b) \tanh^2 \rho \cos 2\phi} \right. \\ &\quad \left. - \tanh^2 \rho (\sqrt{1 + \delta(b)} \cos^2 \phi + \sqrt{1 - \delta(b)} \sin^2 \phi) \right) \simeq 1 + o(\delta^2(b)). \end{aligned} \quad (26)$$

Our MC procedure to generate the freeze-out hadron multiplicities, four-momenta and four-coordinates for central collisions has been described in detail in Ref. [1]. For noncentral collisions, only the generation of the transverse radius r is slightly different, taking place in the azimuthally dependent interval $[0, R(b, \phi)]$.

III. INPUT PARAMETERS AND EXAMPLE CALCULATIONS

A. Model input parameters

First, we summarize the input parameters which control the execution of our MC hadron generator in the case of Bjorken-like and Hubble-like parametrizations, and should be specified for different energies, ion beams and event centralities.

1. Thermodynamic parameters at chemical freeze-out: temperature T^{ch} and chemical potentials per a unit charge $\tilde{\mu}_B, \tilde{\mu}_S, \tilde{\mu}_Q$. As an option, an additional parameter $\gamma_s \leq 1$

takes into account the strangeness suppression according to the partially equilibrated distribution [23, 24]:

$$f_i(p^{*0}; T, \mu_i, \gamma_s) = \frac{g_i}{\gamma_s^{-n_i^s} \exp([p^{*0} - \mu_i]/T) \pm 1}, \quad (27)$$

where n_i^s is the number of strange quarks and antiquarks in a hadron i , p^{*0} is the hadron energy in the fluid element rest frame, $g_i = 2J_i + 1$ is the spin degeneracy factor. Optionally, the parameter γ_s can be fixed using its phenomenological dependence on the temperature and baryon chemical potential [25].

2. Volume parameters: the fireball transverse radius $R(b = 0)$ (determined in central collisions; in noncentral collisions we use the scaling option (8,9) to recalculate $R(b)$ from $R(b = 0)$), the freeze-out proper time τ and its standard deviation $\Delta\tau$ (emission duration) [26].
3. Maximal transverse flow rapidity $\rho_u^{\max}(b = 0)$ for Bjorken-like parametrization in central collisions.
4. Maximal space-time longitudinal rapidity η_{\max} which determines the rapidity interval $[-\eta_{\max}, \eta_{\max}]$ in the collision center-of-mass system. To account for the violation of the boost invariance, we have included in the code an option corresponding to the substitution of the uniform distribution of the space-time longitudinal rapidity η in the interval $[-\eta_{\max}, \eta_{\max}]$ by a Gaussian distribution $\exp(-\eta^2/2\Delta\eta^2)$ with a width parameter $\Delta\eta = \eta_{\max}$ (see, e.g., [20, 27]).
5. Impact parameter range: minimal b_{\min} and maximal b_{\max} impact parameters.
6. Flow anisotropy parameter $\delta(b)$ in Bjorken-like and Hubble-like parametrizations (or $\rho_0(b)$ and $\rho_2(b)$ in the “Blast-Wave” parametrization of Ref. [11]).
7. Coordinate anisotropy parameter $\epsilon(b)$.
8. Thermal freeze-out temperature T^{th} (if single freeze-out is considered, $T^{\text{th}} = T^{\text{ch}}$).
9. Effective chemical potential of π^+ at thermal freeze-out $\mu_{\pi}^{\text{eff th}}$ (0, if single freeze-out is considered).
10. Parameter which enables/disables weak decays.

TABLE I: Model parameters for central Au + Au collisions at $\sqrt{s}_{NN} = 200$ GeV. Chemical freeze-out parameters: $T^{\text{ch}}=0.165$ GeV, $\tilde{\mu}_B=0.028$ GeV, $\tilde{\mu}_S=0.007$ GeV, $\tilde{\mu}_Q = -0.001$ GeV.

T^{th} , GeV	0.165	0.130	0.100
τ , fm/c	7.0	7.2	8.0
$\Delta\tau$, fm/c	2.0	2.0	2.0
$R(b=0)$, fm	9.0	9.5	10.0
$\rho_u^{\text{max}}(b=0)$	0.65	0.9	1.1
$\mu_\pi^{\text{eff th}}$	0.	0.10	0.11

TABLE II: Model parameters for Au + Au collisions at $\sqrt{s}_{NN} = 200$ GeV at different centralities. Chemical freeze-out parameters: $T^{\text{ch}}=0.165$ GeV, $\tilde{\mu}_B=0.028$ GeV, $\tilde{\mu}_S=0.007$ GeV, $\tilde{\mu}_Q = -0.001$ GeV. Thermal freeze-out parameters: $T^{\text{th}}=0.1$ GeV, $\mu_\pi^{\text{eff th}}=0.11$ GeV. Volume parameters determined in the central collisions: $R(b=0)=10.0$ fm, $\tau=8.0$ fm/c, $\rho_u^{\text{max}}(b=0) = 1.1$

centrality	c=0–5 %	c=5–10 %	c=10–20 %	c=20–30 %	c=30–40 %	c=40–60 %
b_{min}/R_A	0.	0.447	0.632	0.894	1.095	1.265
b_{max}/R_A	0.447	0.632	0.894	1.095	1.265	1.549
$\epsilon(b)$	0	0	0	0.1	0.15	0.15
$\delta(b)$	0.05	0.08	0.12	0.25	0.34	0.36

The parameters used to simulate central collisions are given in Table I. The parameters determined in central collisions for $T^{\text{th}}=0.1$ GeV: $\tau=8.0$ fm/c, $R(b=0)=10.$ fm, $\Delta\tau=2.0$ fm/c; $\rho_u^{\text{max}}(b=0) = 1.1$ (3-th column in Table I) were used to simulate Au+Au collisions at $\sqrt{s}_{NN} = 200$ GeV at different centralities. The additional parameters needed only for noncentral collisions are given in Table II.

B. Different chemical and thermal freeze-outs

Since the assumption of a common chemical and thermal freeze-out can hardly be justified (see, e.g., [2]), we consider here a more complicated scenario with different chemical and thermal freeze-outs.

The mean particle numbers \bar{N}_i^{th} at thermal freeze-out can be determined using the following procedure [2]. In our preceding article [1] the temperature and chemical potentials at chemical freeze-out have been fixed by fitting the ratios of the numbers of (quasi)stable particles. The common factor, $V_{\text{eff}}^{\text{ch}}$, and, thus, the absolute particle and resonance numbers was fixed by pion multiplicities. Within the concept of chemically frozen evolution these numbers are assumed to be conserved except for corrections due to decay of some part of short-lived resonances that can be estimated from the assumed chemical to thermal freeze-out evolution time. Then one can calculate the mean numbers of different particles and resonances reaching a (common) thermal freeze-out hypersurface. At a given thermal freeze-out temperature T^{th} these mean numbers can be expressed through the thermal effective volume $V_{\text{eff}}^{\text{th}}$ and the chemical potentials for each particle species μ_i^{th} . The latter can no longer be expressed in the form $\mu_i = \vec{q}_i \vec{\mu}$, which is valid only for chemically equilibrated systems. For a given parametrization of the thermal freeze-out hypersurface, the thermal effective volume $V_{\text{eff}}^{\text{th}}$ (and thus all μ_i^{th}) can be fixed with the help of pion interferometry data.

In practical calculations the particle number density $\rho_i^{\text{eq}}(T, \mu_i)$ is represented in the form of a fast converging series [1]:

$$\rho_i^{\text{eq}}(T, \mu_i) = \frac{g_i}{2\pi^2} m_i^2 T \sum_{k=1}^{\infty} \frac{(\mp)^{k+1}}{k} \exp\left(\frac{k\mu_i}{T}\right) K_2\left(\frac{km_i}{T}\right), \quad (28)$$

where K_2 is the modified Bessel function of the second order, m_i and $g_i = 2J_i + 1$ are the mass and the spin degeneracy factor of particle i respectively.

Using Eq. (28) and the assumption of the conservation of the particle number ratios from the chemical to thermal freeze-out evolution time, we obtain the following ratios for i -particle specie to π^+ :

$$\frac{\rho_i^{\text{eq}}(T^{\text{ch}}, \mu_i)}{\rho_{\pi}^{\text{eq}}(T^{\text{ch}}, \mu_{\pi}^{\text{ch}})} = \frac{\rho_i^{\text{eq}}(T^{\text{th}}, \mu_i^{\text{th}})}{\rho_{\pi}^{\text{eq}}(T^{\text{th}}, \mu_{\pi}^{\text{eff th}})}. \quad (29)$$

The absolute values of particles densities $\rho_i^{\text{eq}}(T^{\text{th}}, \mu_i^{\text{th}})$ are determined by the choice of the free parameter of the model: effective pion chemical potential $\mu_{\pi}^{\text{eff th}}$ at the temperature of thermal freeze-out T^{th} . Assuming for the other particles (heavier then pions) the Boltzmann approximation in Eq. (28) one deduces from Eqs. (28) - (29) the chemical potentials of particles and resonances at thermal freeze-out:

$$\mu_i^{\text{th}} = T^{\text{th}} \ln\left(\frac{\rho_i^{\text{eq}}(T^{\text{ch}}, \mu_i^{\text{ch}})}{\rho_i^{\text{eq}}(T^{\text{th}}, \mu_i = 0)} \frac{\rho_{\pi}^{\text{eq}}(T^{\text{th}}, \mu_{\pi}^{\text{eff th}})}{\rho_{\pi}^{\text{eq}}(T^{\text{ch}}, \mu_{\pi}^{\text{ch}})}\right). \quad (30)$$

The correct way to determine the best set of model parameters would be achieved by fitting all the observables together as it was suggested in Ref. [27], but for our MC-type model it is technically impossible. For the example calculations with our model at RHIC energies we choose $T^{\text{ch}} = 0.165$ GeV and the thermal temperatures as in the analytical models which performed the successful fitting of RHIC data: $T^{\text{th}} = T^{\text{ch}} = 0.165$ GeV (Cracow model [15]) and $T^{\text{th}} = 0.100$ GeV (Blast-Wave model [11]), and some arbitrary intermediate temperature $T^{\text{th}} = 0.130$ GeV. It is well known (see, e.g., [2]) that the pion transverse spectra at thermal freeze-out can be described in two regimes: low temperature and large transverse flow on the one hand, and higher temperature and non-relativistic transverse flow on the other hand (see section III C). The low temperature regime seems to be preferable because the strong transverse flow is expected to describe the large inverse slopes of transverse spectra of the heavy hadrons (especially protons) and small correlation radii obtained at RHIC better [3, 11]. We present the calculated correlation radii in section III E.

In the considered here last version of FASTMC the new table of resonances was included. It contains 360 resonances and stable particles, instead of 85 ones included in the previous versions. This particle table is produced from the SHARE [28] particle table excluding not well established resonances states. The decays of resonances are controlled by its lifetime $1/\Gamma$, where Γ is the width of resonance specified in the particle table, and they occur with the probability density $\Gamma \exp(-\Gamma\tau)$ in the resonance rest frame. Then the decay products are boosted to the reference frame in which the freeze-out hypersurface was defined. Because we need to compare our calculations with data from different experiments we made possible to switch on/off different decays based on their lifetime (i.e. turn on/off weak decays). Only the two- and three-body decays are considered in our model. The branching ratios are also taken from the particle decay table produced from the SHARE decay table [28]. The cascade decays are also possible.

C. m_t -spectra

In Fig. 2 the m_t -spectra measured by the STAR Collaboration [29] at 0–5% centrality are shown for π^+ , K^+ and p in comparison with the model calculations under the assumption of the common chemical and thermal freeze-out at $T^{\text{th}} = T^{\text{ch}} = 0.165$ GeV (Fig. 2(a)) and under the assumption that the thermal freeze-out at $T^{\text{th}} = 0.100, 0.130$ GeV occurs after

the chemical one (Fig. 2(b, c)).

The correction on weak decays was introduced by the STAR Collaboration in pion spectra only [29]. It was approximately 12% and was estimated from the measured K_s^0 and Λ decays. In Ref. [29] the STAR Collaboration doesn't introduce the weak decay correction in proton spectra. To reproduce the STAR weak decay correction procedure, we excluded pions from K_s^0 and Λ decays from pions m_t -spectra in Fig. 2. The contribution of weak decays in the simulated proton spectra can be estimated from Fig. 2 by comparison of the solid lines (protons from K_s^0 and Λ decays are included) and the dashed lines (without contribution of protons from the weak decays). The model parameters at different temperatures are presented in Table I. The parameters were optimized this way to obtain the good description of the pion m_t -spectra and the correlation radii. The best description of the m_t -spectra was achieved at $T^{\text{th}} = 0.100$ GeV (Fig. 2(c)).

The same set of parameters $T, \rho_u^{\text{max}}, R$ and τ which was determined for central collisions (Table I) was used for noncentral ones. The additional parameters of the model for non-central collisions were coordinate and momentum asymmetries: ϵ and δ (Table II). At the freeze-out moment we consider them as free parameters because we do not trace the evolution here. The influence of the choice of ϵ and δ on m_t -spectra averaged over azimuthal angle φ is negligible. The decrease of the effective volume in noncentral collisions (Eq. 20) due to nonzero values of ϵ and δ allows us to obtain the correct absolute normalization of m_t -spectra without introduction of the additional parameters. In Fig. 3 the m_t -spectra measured by the STAR Collaboration [29] are shown for π^+ , K^+ and p at centralities: 0 – 5%, 5 – 10%, 10 – 20%, 20 – 30%, 30 – 40%, 40 – 50% in comparison with the model calculations which assume that the thermal freeze-out at $T^{\text{th}} = 0.1$ GeV occurs after the chemical one (solid lines). It appears that the procedure described in section II allows one to achieve the absolute normalization of pion spectra correct within $\sim 13\%$.

D. Elliptic flow

Following a standard procedure [30, 31] we make a Fourier expansion of the hadron distribution in the azimuthal angle φ at mid-rapidity:

$$\frac{dN}{d^2p_t dy} = \frac{dN}{2\pi p_t dp_t dy} (1 + 2v_2 \cos 2\varphi + 2v_4 \cos 4\varphi + \dots). \quad (31)$$

The elliptic flow coefficient, v_2 , is defined as the second order Fourier coefficient,

$$v_2 = \frac{\int_0^{2\pi} d\varphi \cos 2(\varphi - \psi_R) \frac{d^3 N}{dy d\varphi p_t dp_t}}{\int_0^{2\pi} d\varphi \frac{d^3 N}{dy d\varphi p_t dp_t}}, \quad (32)$$

where ψ_R is the reaction plane angle (in our generation $\psi_R = 0$), y and p_t are the rapidity and transverse momentum of particle under consideration, respectively.

The value of v_2 is an important signature of the physics occurring in heavy ion collisions. According to the typical hydrodynamic scenario shown in Fig. 1, the elliptic flow is generated mainly during the high density phase of the fireball evolution. The system driven by the internal pressure gradients expands more strongly in its short direction (into the direction of the impact parameter x in Fig. 1, which is chosen as a “positive” direction) than in the perpendicular one (“negative” direction, y in Fig. 1) where the pressure gradients are smaller. Figure 1 illustrates qualitatively that the initial spacial anisotropy of the system disappears during the evolution, while the momentum anisotropy grows. The developing of strong flow observed at RHIC requires a short time scale and large pressure gradients, which are characteristics of a strongly interacting system. The reason for the generation of v_2 at the early times is that the system should be hot and dense, when the system cools and become less dense the developing of the large pressure gradients becomes impossible. The elliptic flow coefficient, v_2 , depends on the transverse momentum p_t , the impact parameter b or centrality, as well as, the type of the considered particle. All these dependencies have been measured at RHIC [32].

The p_t -dependence of v_2 measured by the STAR Collaboration [32] for charged particles at centralities: 0 – 5%, 5 – 10%, 10 – 20%, 20 – 30%, 30 – 40%, 40 – 60% is shown in Fig. 4 in comparison with our MC calculations obtained with the optimal model parameters from Table II. The calculations were performed under the assumption that thermal freeze-out at $T^{\text{th}} = 0.1$ GeV occurs after the chemical one at $T^{\text{th}} = 0.165$ GeV.

The calculations under the assumption of the common chemical and thermal freeze-out at $T^{\text{th}} = T^{\text{ch}} = 0.165$ GeV demonstrate not so good agreement with the experimental data at small $p_t < 0.4$ GeV/ c for the centralities larger than 20%; irrespective of the choice of ϵ and δ one cannot get a satisfactory description in the whole p_t -range (see e.g. Fig. 5).

E. Correlation radii

The parameters of the model presented in Table I were optimized to obtain the best description of the pion m_t -spectra and the correlation radii in the following cases: under the assumption of the common chemical and thermal freeze-out at $T^{\text{th}} = T^{\text{ch}} = 0.165$ GeV and under the assumption that the thermal freeze-out at $T^{\text{th}} = 0.100, 0.130$ GeV occurs after the chemical one. In Fig. 6 the fitted correlation radii R_{out} , R_{side} and R_{long} are compared with those measured by the STAR Collaboration [5]. The three-dimensional correlation function was fitted with the standard Gaussian formula:

$$CF(p_1, p_2) = 1 + \lambda \exp(-R_{\text{out}}^2 q_{\text{out}}^2 - R_{\text{side}}^2 q_{\text{side}}^2 - R_{\text{long}}^2 q_{\text{long}}^2), \quad (33)$$

where $\vec{q} = \vec{p}_1 - \vec{p}_2 = (q_{\text{out}}, q_{\text{side}}, q_{\text{long}})$ is the relative three-momentum of two identical particles with four-momenta p_1 and p_2 . The form of Eq. (33) assumes azimuthal symmetry of the production process [33]. Generally, e.g., in the case of the correlation analysis with respect to the reaction plane, all three cross terms $q_i q_j$ can be significant [27]. We will consider this case below. We choose the longitudinal co-moving system (LCMS) as the reference frame [34]. In LCMS each pair is emitted transverse to the reaction axis so that the pair rapidity vanishes. The parameter λ measures the correlation strength.

The regime with the large temperature $T^{\text{th}} = T^{\text{ch}} = 0.165$ GeV was tested in Ref. [1]. We have repeated this test here with the new resonances table and the additional parameter $\Delta\tau$ (Fig. 6(a), dashed line). We have found that these modifications lead to a better description of the correlation radii. In Fig. 6(a, bottom) (dashed line) the intercept λ is larger than the experimental one, but taking into account the secondary pions from the weak decays essentially improves the description of the λ (Fig. 6(a, bottom), solid line).

In Fig. 6(b, c) we consider the lower thermal freeze-out temperatures: 0.130, 0.100 GeV. The secondary pions coming from the weak decays were taken into account.

It is worth to note a good description of the correlation radii (within $\sim 10\%$ accuracy) altogether with the absolute value of the m_t spectra in the scenario with a low temperature thermal freeze-out of chemically frozen hadron-resonance gas. There are three important reasons for this success. First, a relatively small (compared with dynamic models) effective volume of the system $\sim \tau R^2$ that reduces the correlation radii. Second, relatively large transverse flow in the model that further reduces the radii. Third, rather large effective

pion chemical potential which is needed to describe the absolute value of the pion spectra at relatively small effective volumes; it reduces correlation radii at small p_t and so makes their m_t behavior flatter. This reduction happens due to vanishing of the homogeneity length of Bose-Einstein distribution for low- p_t pions when the pion chemical potential approaches the pion mass (see also Ref. [35] for the analysis of the reduction of the pion correlation radii near the point of the Bose-Einstein condensation in static systems). We do not consider here the question whether such conditions could be realized in realistic dynamical models.

It should be noted that the description of the k_t -dependence of the correlation radii has been achieved within $\sim 10\%$ accuracy for all three considered thermal temperatures: $T^{\text{th}} = 0.165, 0.130, 0.100$ GeV. However, at lower temperatures there is more flexibility in the simultaneous description of particle spectra and correlations because the effective volume isn't strictly fixed as it is in the case of the single freeze-out ($T^{\text{th}} = T^{\text{ch}} = 0.165$ GeV). In present work, we have not attempted to fit the model parameters ($T^{\text{th}}, R, \tau, \mu_\pi^{\text{eff th}}$) since it is rather complicated task requiring a lot of computer time. We have performed only example calculations with several sets of the parameters.

In noncentral collisions the measurement of azimuthally sensitive correlation radii provides the additional information about the source shape. For the corresponding femtoscopy formalism with respect to the reaction plane see, e.g., [18, 27]. In the absence of azimuthal symmetry, the three additional cross terms contribute to the Gaussian parametrization of the correlation function in Eq. (33):

$$CF(p_1, p_2) = 1 + \lambda \exp(-R_o^2 q_{\text{out}}^2 - R_s^2 q_{\text{side}}^2 - R_l^2 q_{\text{long}}^2 - 2R_{\text{os}}^2 q_{\text{out}} q_{\text{side}} - 2R_{\text{ol}}^2 q_{\text{out}} q_{\text{long}} - 2R_{\text{sl}}^2 q_{\text{side}} q_{\text{long}}). \quad (34)$$

In the boost-invariant case, the transverse-longitudinal cross terms R_{ol}^2 and R_{sl}^2 vanish in the LCMS frame, while the important out-side R_{os}^2 cross term is present.

In the Gaussian approximation, the radii in the Eq. (34) are related to space-time variances via the set of equations [18, 27]:

$$\begin{aligned} R_s^2 &= 1/2(\langle \tilde{x}^2 \rangle + \langle \tilde{y}^2 \rangle) - 1/2(\langle \tilde{x}^2 \rangle - \langle \tilde{y}^2 \rangle) \cos(2\Phi) - \langle \tilde{x}\tilde{y} \rangle \sin(2\Phi), \\ R_o^2 &= 1/2(\langle \tilde{x}^2 \rangle + \langle \tilde{y}^2 \rangle) + 1/2(\langle \tilde{x}^2 \rangle - \langle \tilde{y}^2 \rangle) \cos(2\Phi) + \langle \tilde{x}\tilde{y} \rangle \sin(2\Phi) \\ &\quad - 2\beta_\perp (\langle \tilde{t}\tilde{x} \rangle \cos(\Phi) + \langle \tilde{t}\tilde{y} \rangle \sin(\Phi)) + \beta_\perp^2 \langle \tilde{t}^2 \rangle, \\ R_l^2 &= \langle \tilde{z}^2 \rangle - 2\beta_l \langle \tilde{t}\tilde{z} \rangle + \beta_l^2 \langle \tilde{t}^2 \rangle, \\ R_{\text{os}}^2 &= \langle \tilde{x}\tilde{y} \rangle \cos(2\Phi) - 1/2(\langle \tilde{x}^2 \rangle - \langle \tilde{y}^2 \rangle) \sin(2\Phi) + \beta_\perp (\langle \tilde{t}\tilde{x} \rangle \sin(\Phi) - \langle \tilde{t}\tilde{y} \rangle \cos(\Phi)), \end{aligned} \quad (35)$$

where $\beta_l = k_z/k^0$, $\beta_\perp = k_\perp/k^0$ and $\Phi = \angle(\vec{k}_\perp, \vec{b})$ is the azimuthal angle of the pair three-momentum \vec{k} with respect to the reaction plane z - x determined by the longitudinal direction and the direction of the impact parameter vector $\vec{b} = (x, 0, 0)$; the space-time coordinates \tilde{x}^μ are defined relative to the effective source center $\langle x^\mu \rangle$: $\tilde{x}^\mu = x^\mu - \langle x^\mu \rangle$. The averages are taken with the source emission function $S(t, \vec{x}, k)$, [18]:

$$\langle f(t, \vec{x}) \rangle = \frac{\int d^4x f(t, \vec{x}) S(t, \vec{x}, k)}{\int d^4x S(t, \vec{x}, k)}. \quad (36)$$

The illustrative calculations of the correlation radii as a function of the azimuthal angle Φ were done with the following fast MC parameters: $T^{\text{th}} = 0.1$ GeV, $\rho_u^{\text{max}}(b = 0) = 1.0$; $R(b = 0) = 11.5$ fm, $\tau = 7.5$ fm/ c , $\Delta\tau = 0$ fm/ c , $\epsilon = 0.1$ and $\delta = 0.25$. The azimuthal dependence of the correlation radii in different k_t intervals is shown in Fig. 7.

The R_s^2 oscillates downward, in the same phase as "RHIC" source extended out of plane [36], which means the larger sideward radius viewed from the x -direction (in the reaction plane), than from y -direction (out-of plane). The source has small coordinate asymmetry $\epsilon = 0.1$, it is almost round (as in Fig. 1 step 3), however the emission zone, or "homogeneity region", varies with Φ because of the non-isotropic flow.

IV. CONCLUSIONS

We have developed a MC simulation procedure and the corresponding C++ code, that allows a fast realistic description of multiple hadron production both in central and noncentral relativistic heavy ion collisions. A high generation speed and an easy control through input parameters make our MC generator code particularly useful for detector studies. As options, we have implemented two freeze-out scenarios with coinciding and with different chemical and thermal freeze-outs. We have compared the RHIC experimental data with our MC generation results obtained within the single and separated freeze-out scenarios with Bjorken-like freeze-out surface parameterization.

Fixing the temperatures of the chemical and thermal freeze-out at 0.165 GeV and 0.100 GeV respectively, and, using the same set of the model parameters as for the central collisions, we have described single particle spectra at different centralities with the absolute normalization correct within $\sim 13\%$.

The comparison of the RHIC v_2 measurements with our MC generation results shows

that the scenario with two separated freeze-outs is more favorable for the description of the p_t -dependence of the elliptic flow.

The description of the k_t -dependence of the correlation radii has been achieved within $\sim 10\%$ accuracy. The experimentally observed values of the correlation strength parameter λ has been reproduced due to the account of the weak decays.

The analysis of the azimuthal dependence of the correlation radii indicates that the source considered in the model oscillates downward, in the same phase as "RHIC" source extended out of plane.

The achieved understanding of the reasons leading to a good simultaneous description of particle spectra, elliptic flow and femtosopic correlations within the considered simple model could be useful for building of the complete dynamic picture of the matter evolution in A+A collisions.

Acknowledgments

We would like to thanks A. Kisiel, W. Broniowski and W. Florkowski for the permission to use the particle data table from SHARE used in their THERMINATOR code. We would like to thank Eu. Zabrodin, B.V. Batyunia and L.I. Sarycheva for useful discussions. The research has been carried out within the scope of the ERG (GDRE): Heavy ions at ultra-relativistic energies - a European Research Group comprising IN2P3/CNRS, Ecole des Mines de Nantes, Universite de Nantes, Warsaw University of Technology, JINR Dubna, ITEP Moscow and Bogolyubov Institute for Theoretical Physics NAS of Ukraine. The investigations have been partially supported by the IRP AVOZ10480505, by the Grant Agency of the Czech Republic under Contract No. 202/07/0079 and by the grant LC07048 of the Ministry of Education of the Czech Republic and by Award No. UKP1-2613-KV-04 of the U.S. Civilian Research and Development Foundation (CRDF) and Fundamental Research State Fund of Ukraine, Agreement No. F7/209-2004 and also by Award of Physics and Astronmics Division of NASU /017U000396 (19.12.06), Fundamental Research State Fund of Ukraine, Agreement No. F25/718-2007 and Bilateral award DLR(Germany)-MESU (Ukraine) for UKR 06/008

Project, and by grant N 08-02-91001-CERN-a of Russian Foundation for Basic Research.

- [1] N.S. Amelin, R. Lednicky, T.A. Pocheptsov, I.P. Lokhtin, L.V. Malinina, A.M. Snigirev, Iu.A. Karpenko, and Yu.M. Sinyukov, Phys. Rev. C **74**, 064901 (2006).
- [2] S.V. Akkelin, P. Braun-Munzinger, and Yu.M. Sinyukov, Nucl. Phys. **A710**, 439 (2002).
- [3] M.S. Borysova, Yu.M. Sinyukov, S.V. Akkelin, B. Erasmus, and Iu.A. Karpenko, Phys. Rev. C **73**, 024903 (2006).
- [4] C. Adler *et al.* (STAR Collaboration), Phys. Rev. Lett. **87**, 182301 (2001).
- [5] J. Adams *et al.* (STAR Collaboration), Phys. Rev. C **71**, 044906 (2005).
- [6] P.F. Kolb, J. Sollfrank, and U.W. Heinz, Phys. Lett. **B459**, 667 (1999).
- [7] D. Hardtke and S.A. Voloshin, Phys. Rev. C **61**, 024905 (2000).
- [8] R.J.M. Snellings, A.M. Poskanzer, and S.A. Voloshin, nucl-ex/9904003.
- [9] M. Bleicher and H. Stoecker, Phys. Lett. **B526**, 309 (2002).
- [10] B. Zhang, C.M. Ko, B.A. Li, and Z.W. Lin, Phys. Rev. C **61**, 067901 (2000); Z.W. Lin, S. Pal, C.M. Ko, B.A. Li, and B. Zhang, Phys. Rev. C **64**, 011902 (2001).
- [11] F. Retiere and M.A. Lisa, Phys. Rev. C **70**, 044907 (2004).
- [12] A. Kisiel, T. Taluc, W. Broniowski, and W. Florkowski, Comput. Phys. Commun. **174**, 669 (2006).
- [13] W. Florkowski, W. Broniowski, A. Kisiel, and J. Pluta, Acta Phys. Polon. **B37**, 3381 (2006).
- [14] M. Csanad, T. Csörgö and B. Lörstad, Nucl. Phys. **A 742**, 80 (2004).
- [15] W. Florkowski and W. Broniowski, Acta. Phys. Pol. **35**, 2855 (2004).
- [16] J.D. Bjorken, Phys. Rev. D **27**, 140 (1983).
- [17] P. Huovinen, P.F. Kolb, U. Heinz, P.V. Ruuskanen, and S.A. Voloshin, Phys. Lett. **B503**, 58 (2001).
- [18] U.A. Wiedemann, Phys. Rev. C **57**, 266 (1998).
- [19] W. Broniowski, A. Baran, and W. Florkowski, AIP Conf. Proc. **660**, 185 (2003).
- [20] I.P. Lokhtin and A.M. Snigirev, Eur. Phys. J. C **45**, 211 (2006).
- [21] U.W. Heinz and S.M.H. Wong, Phys. Rev. C **66**, 014907 (2002).
- [22] T. Csörgö and B. Lörstad, Phys. Rev. C **54**, 1390 (1996).
- [23] G.D. Yen, M.I. Gorenstein, W. Greiner, and S.N. Yang, Phys. Rev. C **56**, 2210 (1997).

- [24] J. Rafelski, Phys. Lett. **B262**, 333 (1981).
- [25] F. Becattini, J. Manninen, and M. Gazdzicki, Phys. Rev. C **73**, 044905 (2006).
- [26] L.V. Bravina et al., Nucl. Phys. A **698**, 383 (2002).
- [27] U.A. Wiedemann and U. Heinz, Phys. Rept. **319**, 145 (1999).
- [28] G. Torrieri et al., nucl-th/0404083 (2004).
- [29] J. Adams *et al.* (STAR Collaboration), Phys. Rev. Lett. **92**, 112301 (2004).
- [30] S. Voloshin and Y. Zang, Z. Phys. C **70**, 665 (1996).
- [31] A.M. Poskanzer and S.A. Voloshin, Phys. Rev. C **58**, 1671 (1998).
- [32] J. Adams *et al.* (STAR Collaboration), Phys. Rev. C **72**, 014904 (2005).
- [33] M.I. Podgoretskii, Sov. J. Nucl. Phys. **37**, 272 (1983).
- [34] T. Csörgö and S. Pratt, Proc. of the Workshop on Heavy Ion Physics, KFKI-1991-28/A, 75.
- [35] R. Lednicky, V. Lyuboshitz, K. Mikhailov, Yu. Sinyukov, A. Stavinsky and B. Erazmus, Phys. Rev. C **61** 034901 (2000).
- [36] J. Adams *et al.* (STAR Collaboration), Phys. Rev. Lett. **93**, 012301 (2004).

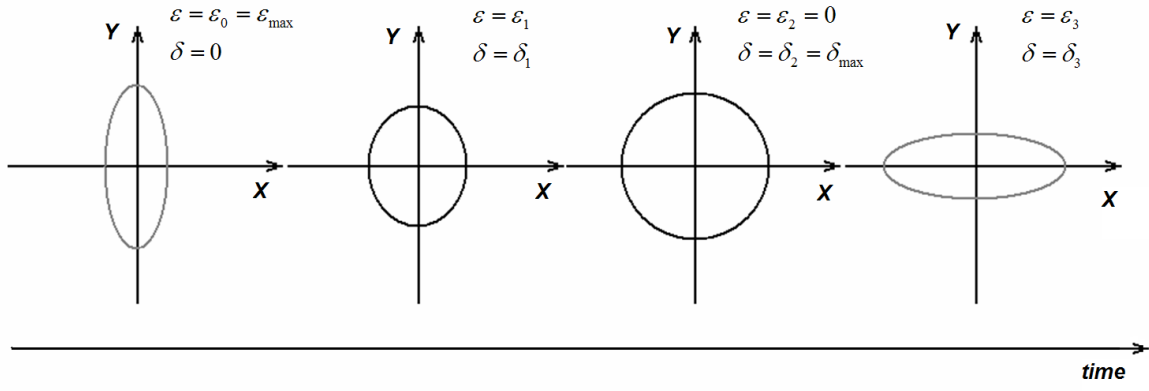


FIG. 1: The typical hydrodynamic evolution scenario.

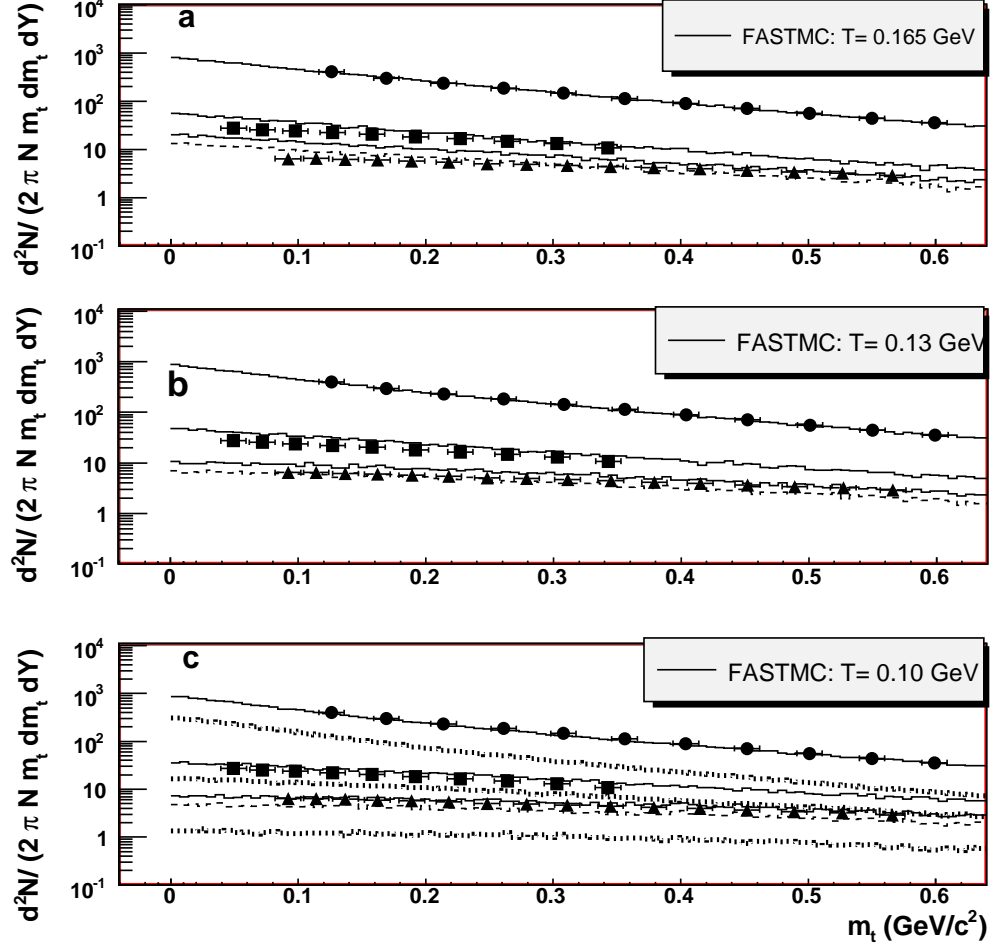


FIG. 2: m_t -spectra (in c^4/GeV^2) measured by the STAR Collaboration [29] for π^+ (circles), K^+ (squares) and p (up-triangles) at 0 – 5% centrality in comparison with the model calculations at $T^{\text{th}} = 0.165(a), 0.130(b), 0.100(c)$ GeV, with the parameters from Table I, for protons weak decays are taken into account (solid lines); for protons weak decays are not taken into account (dashed lines). The direct π^+ , K^+ and p contributions are shown on (c) by dotted lines.

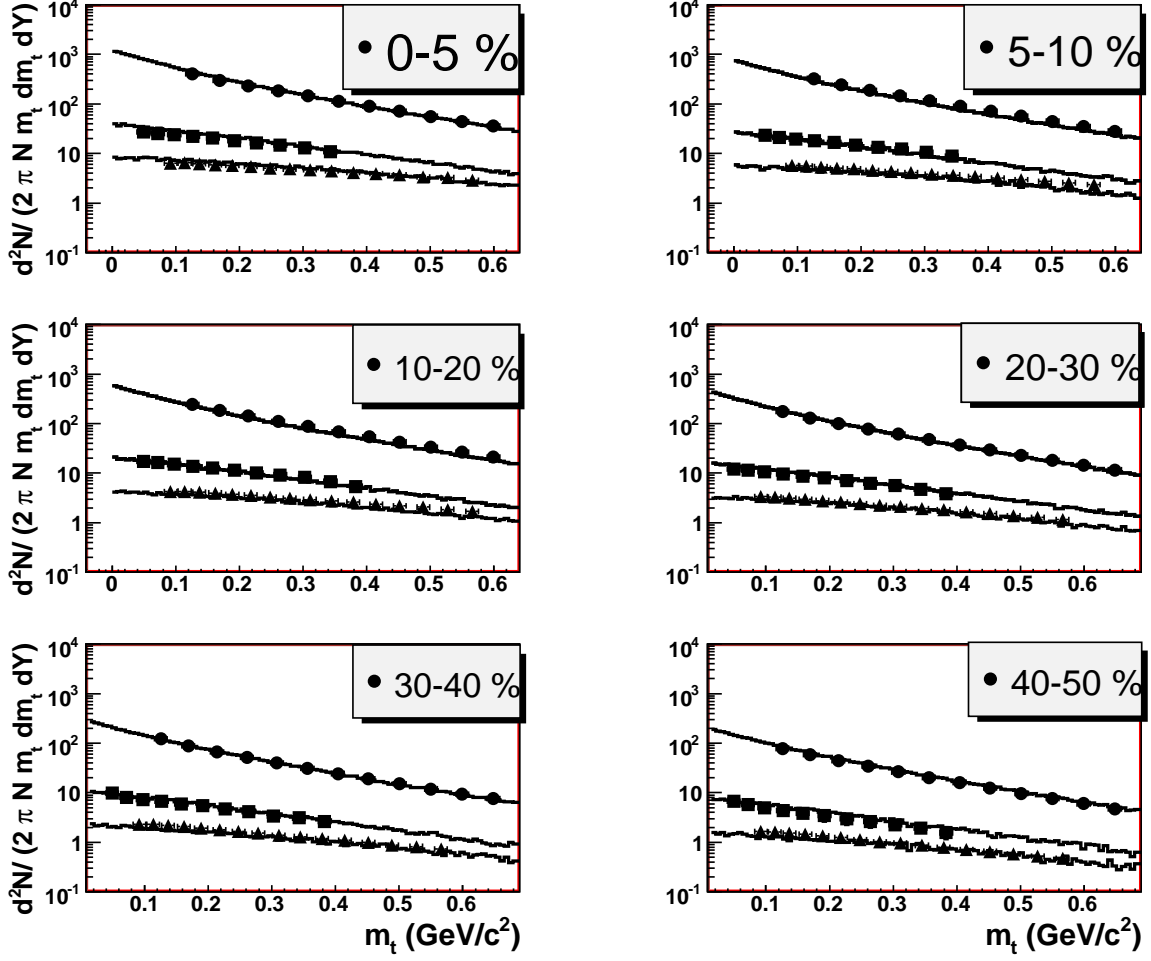


FIG. 3: m_t -spectra (in c^4/GeV^2) measured by the STAR Collaboration [29] for π^+ (circles), K^+ (squares) and p (up-triangles) at different centralities in comparison with our fast MC calculations at $T^{\text{th}} = 0.100$ GeV (solid lines) with the parameters from Table I and Table II.

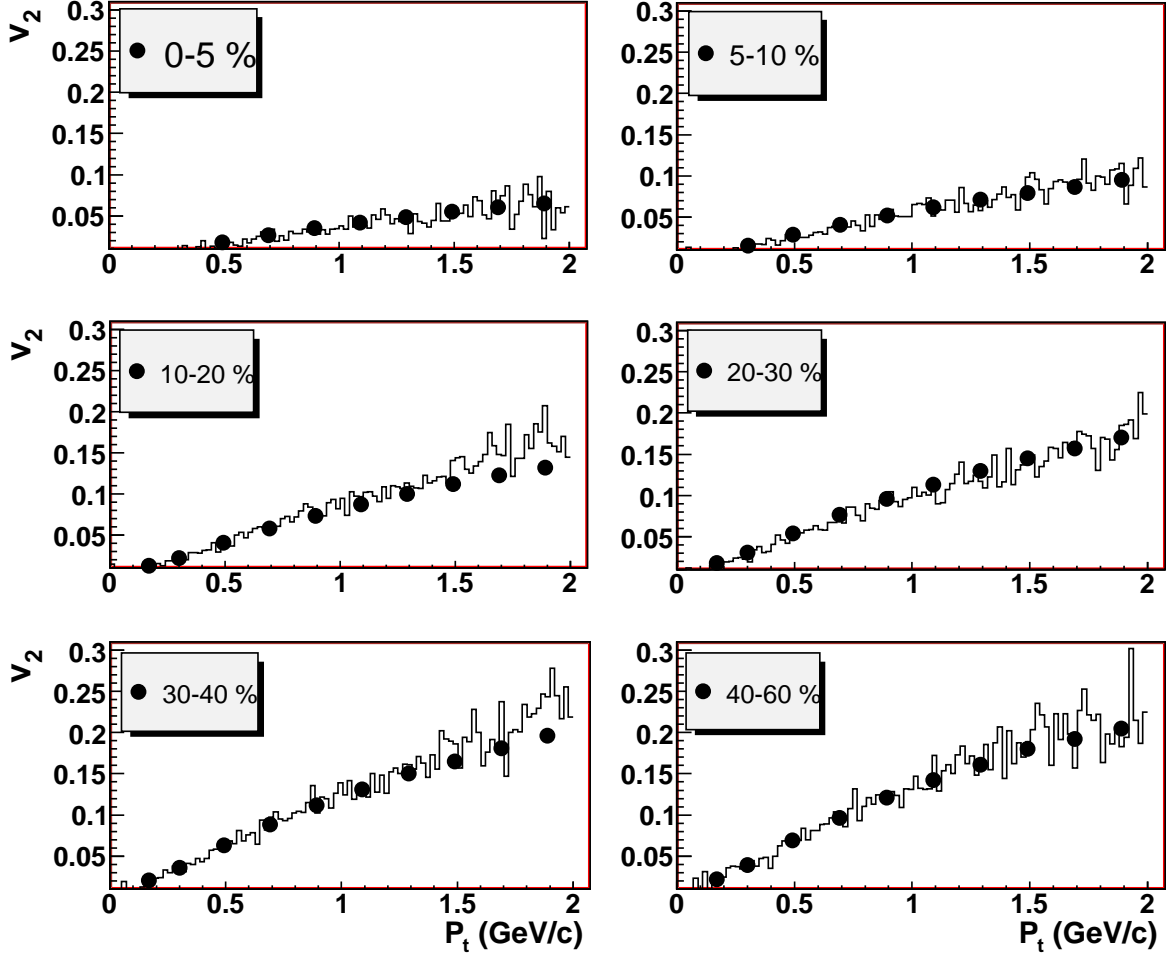


FIG. 4: The p_t -dependence of v_2 measured by the STAR Collaboration [32] (points) for charged particles at different centralities in comparison with our fast MC calculations at $T^{\text{th}} = 0.100$ GeV (solid line) with the parameters from Table I and Table II.

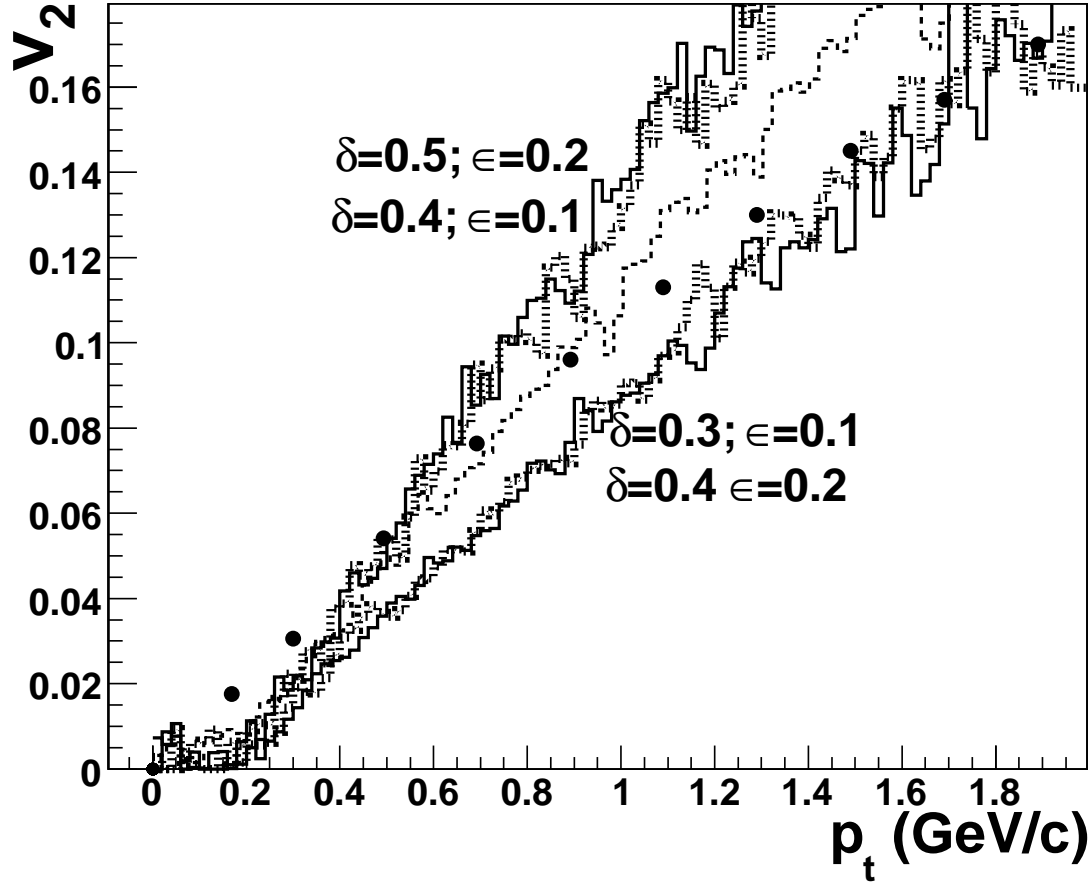


FIG. 5: The p_t -dependence of v_2 measured by the STAR Collaboration [32] (points) for charged particles at centrality 20 – 30% in comparison with our fast MC calculations under assumption of the single freeze-out at $T^{\text{th}} = T^{\text{ch}} = 0.165$ GeV. The different sets of coordinate and momentum assymetries parameters were tried: $\epsilon = 0.1$, $\delta = 0.3$ (solid line), $\epsilon = 0.2$, $\delta = 0.4$ (dotted line), $\epsilon = 0.1$, $\delta = 0.4$ (solid line), $\epsilon = 0.2$, $\delta = 0.5$ (dotted line), $\epsilon = 0.15$, $\delta = 0.4$ (dashed line)

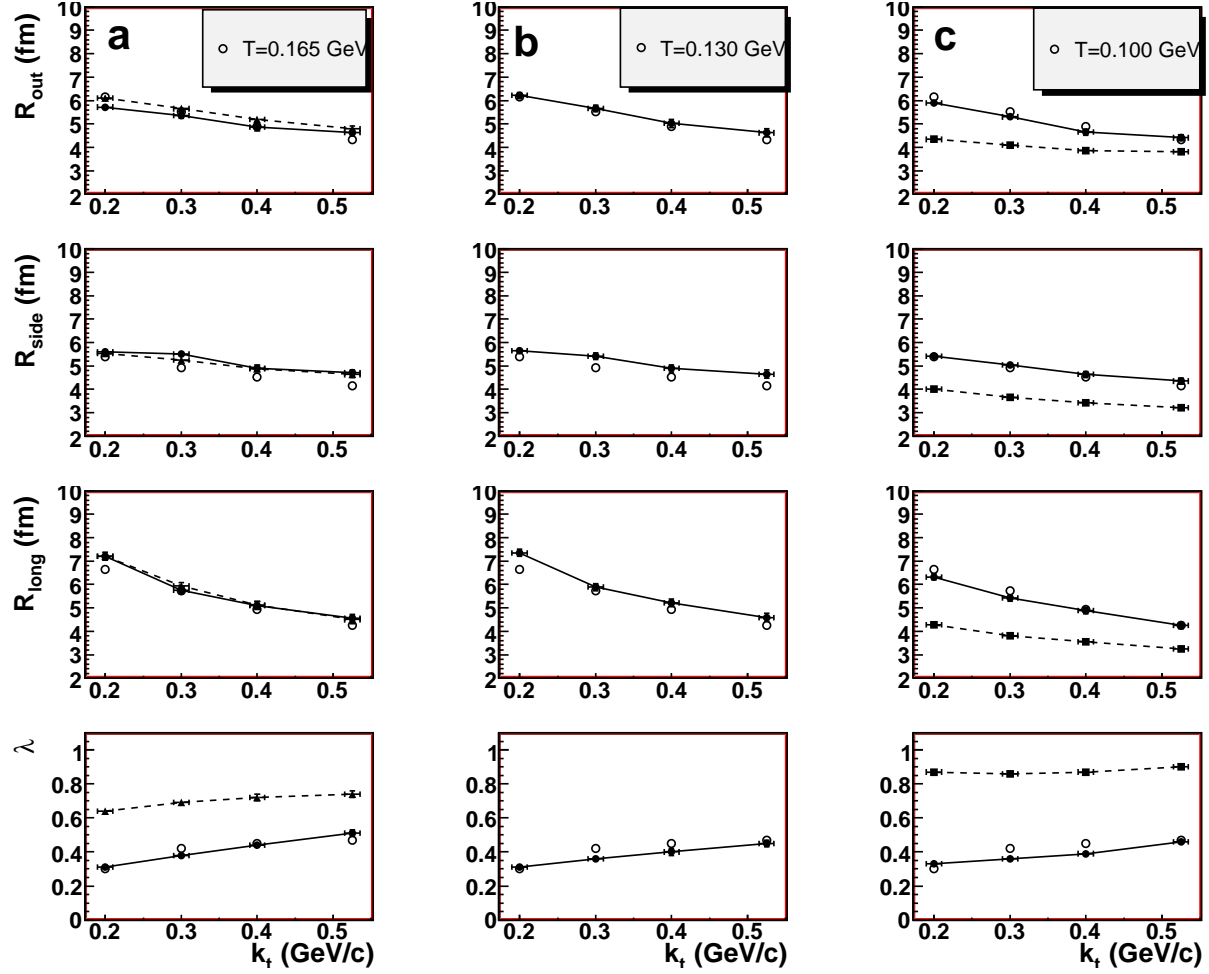


FIG. 6: The π^+ correlation radii at mid-rapidity in central Au+Au collisions at $\sqrt{s_{NN}} = 200$ GeV from the STAR experiment [5] (open circles) and MC calculations within the Bjorken-like model with the parameters presented in Table I in different intervals of the pair transverse momentum k_t . The full calculation with resonances (a), (b). (a) single freeze-out $T^{ch} = T^{th} = 0.165$ GeV, no weak decays (dashed line), with weak decays (solid line); (b) thermal freeze-out at $T^{th} = 0.130$ GeV occurs after the chemical one, weak decays are taken into account (solid line); (c) the full calculation with resonances, weak decays are taken into account at $T^{th} = 0.100$ GeV (solid line), the direct pions only (dotted lines).

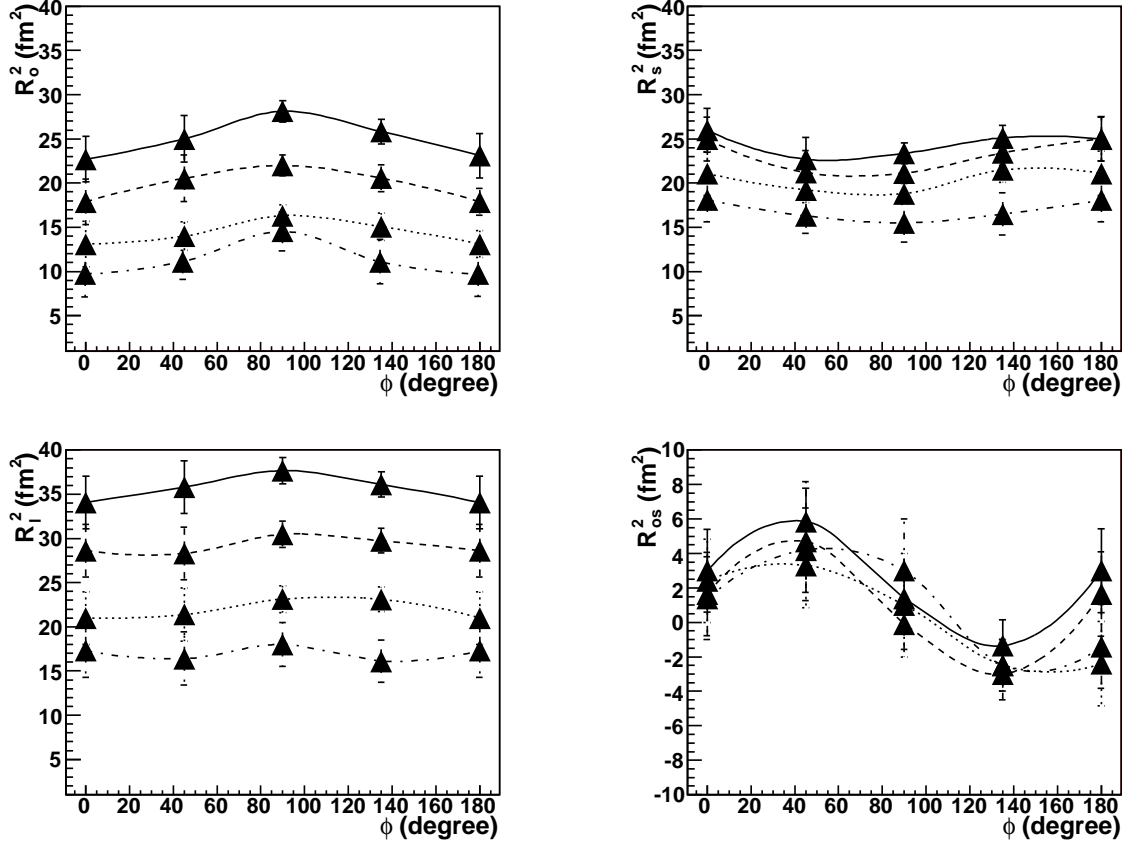


FIG. 7: Simulated with FASTMC squared correlation radii versus the azimuthal angle Φ of the $\pi^+\pi^+$ pair with respect to the reaction plane, 20-30 % centrality events in k_T (GeV/ c) intervals: $0.15 < k_T < 0.25$ (solid line), $0.25 < k_T < 0.35$ (dashed line), $0.35 < k_T < 0.45$ (dotted line), $0.45 < k_T < 0.60$ (dotted-dashed line). simulation was done with the special set of parameters: $T^{\text{th}} = 0.1$ GeV, $\rho_u^{\text{max}}(b = 0) = 1.0$; $R(b = 0) = 11.5$ fm, $\tau = 7.5$ fm/ c , $\Delta\tau = 0$. fm/ c , $\epsilon = 0.1$ and $\delta = 0.25$, weak decays were not taken into account.